Wang et al. *Zool. Res.* 2023, 44(4): 712−724
https://doi.org/10.24272/j.issn.2095-8137.2022.473

ZR | Zoological Research

Article Open Access

Scopolamine causes delirium-like brain network dysfunction and reversible cognitive impairment without neuronal loss

Qing Wang[1,#], Xiang Zhang[1,#], Yu-Jie Guo[1], Ya-Yan Pang[2], Jun-Jie Li[2], Yan-Li Zhao[1], Jun-Fen Wei[1], Bai-Ting Zhu[1], Jing-Xiang Tang[1], Yang-Yang Jiang[1], Jie Meng[1], Ji-Rong Yue[1,*], Peng Lei[1,*]

[1] *Department of Geriatrics and State Key Laboratory of Biotherapy*, *National Clinical Research Center for Geriatrics*, *West China Hospital*, *Sichuan University*, *Chengdu*, *Sichuan* 610041, *China*

[2] *Pediatric Research Institute*, *Ministry of Education Key Laboratory of Child Development and Disorders*, *National Clinical Research Center for Child Health and Disorders*, *Chongqing Key Laboratory of Translational Medical Research in Cognitive Development and Learning and Memory Disorders*, *Children's Hospital of Chongqing Medical University*, *Chongqing* 400014, *China*

ABSTRACT

Delirium is a severe acute neuropsychiatric syndrome that commonly occurs in the elderly and is considered an independent risk factor for later dementia. However, given its inherent complexity, few animal models of delirium have been established and the mechanism underlying the onset of delirium remains elusive. Here, we conducted a comparison of three mouse models of delirium induced by clinically relevant risk factors, including anesthesia with surgery (AS), systemic inflammation, and neurotransmission modulation. We found that both bacterial lipopolysaccharide (LPS) and cholinergic receptor antagonist scopolamine (Scop) induction reduced neuronal activities in the delirium-related brain network, with the latter presenting a similar pattern of reduction as found in delirium patients. Consistently, Scop injection resulted in reversible cognitive impairment with hyperactive behavior. No loss of cholinergic neurons was found with treatment, but hippocampal synaptic functions were affected. These findings provide further clues regarding the mechanism underlying delirium onset and demonstrate the successful application of the Scop injection model in mimicking delirium-like phenotypes in mice.

Keywords: Delirium; Scopolamine; Cholinergic neuron; Neuronal activity; Brain network

INTRODUCTION

Delirium is an acute brain dysfunction syndrome characterized by a fluctuating level of disturbance in attention and awareness and additional cognitive dysfunction, which often develops in elderly patients during hospitalization or severe illness (Association American Psychiatric, 2013; Inouye et al., 2014; Oh et al., 2017). Over 30% of critically ill patients develop delirium, accompanied by an increased risk of cognitive decline and dementia (Krewulak et al., 2018; Salluh et al., 2015). At present, delirium can only be managed symptomatically, with no cure currently available. The administration of antipsychotic medication for the treatment of delirium in hospitalized patients does not result in noticeable improvements, while nonpharmacological interventions have become commonly used in clinical practice to produce substantial benefits by targeting multiple risk factors associated with delirium (Goldberg et al., 2020; Neufeld et al., 2016). Leading factors that trigger delirium include surgery and anesthesia, medications (e.g., anticholinergics and benzodiazepines), dehydration, psychological stress, and systemic inflammatory insults. However, their underlying molecular pathways are poorly understood.

Several animal models have been developed to mimic delirium based on individual risk factors (Abraham & Johnson, 2009; Peng et al., 2016; Qiu et al., 2016a). For example, simple abdominal operation under prolonged anesthesia has been used to induce typical postoperative delirium in animals (Peng et al., 2016). In accordance with the inflammation hypothesis, peripheral inflammatory stimulation with lipopolysaccharide (LPS) has been applied to elicit profound immune responses in the brains of mice by microglial activation (Cerejeira et al., 2010). Single-dose LPS is also known to induce chronic neuroinflammation with neurodegeneration, mimicking executive dysfunction associated with intensive care unit-related delirium (Abraham & Johnson, 2009; Zivkovic et al., 2015). In addition, pharmacologically induced delirium has also been established

Received: 05 March 2023; Accepted: 05 June 2023; Online: 12 June 2023
Foundation items: This work was supported by the National Natural Science Foundation of China (82071191, 82001129), Natural Science Foundation of Sichuan Province (2022NSFSC1509), National Clinical Research Center for Geriatrics of West China Hospital (Z2021LC001), and West China Hospital 1.3.5 Project for Disciplines of Excellence (ZYYC20009)

[#]Authors contributed equally to this work

*Corresponding authors, E-mail: yuejirong11@hotmail.com; peng.lei@scu.edu.cn

using “deliriant” hallucinogenic drugs (Itil & Fink, 1966; Rozzini et al., 1988), including cholinergic antagonists such as atropine and scopolamine (Scop) (Lakstygal et al., 2019). In rodents and zebrafish, atropine and Scop are known to impair stimulus sensitivity, sensory discrimination, vision, and behavioral patterning, resulting in a delirium-like state (Qiu et al., 2016a; Trzepacz et al., 1992).

However, the extent to which these animal models can recapitulate delirium and the ability to differentiate delirium-like phenotypes from potential side effects of drugs and procedures remain uncertain. In the case of animal models established through anesthesia and surgery (AS), the cognitive deficits that arise could potentially be attributed to postoperative cognitive decline (POCD) caused by prolonged anesthesia (Chan et al., 2013; Li et al., 2021). Moreover, the sedative effects and mood disorders induced by the administration of LPS may interfere with cognitive function assessment (O’Connor et al., 2009; Van Den Biggelaar et al., 2007). Furthermore, the phenotypes induced by the application of Scop may not exclusively represent delirium, as Scop is also used to mimic other disorders with cognitive impairment, such as Alzheimer’s disease (AD) (Chen & Yeong, 2020). Delirium affects multiple brain regions, and the integrity of the brain network is compromised under a delirium state (Choi et al., 2012; Fleischmann et al., 2019; Oh et al., 2019). In the current study, we evaluated delirium mouse models by mapping the neuronal activity of the brain network and conducting behavioral tests. We performed comparative analysis of AS-, LPS-, and Scop-induced delirium models, and investigated their potential delirium-like phenotypes. Furthermore, to gain insights into the pathogenesis of delirium, we evaluated the expression of proteins associated with synaptic functions in these models. This study may provide clues for improving the replication of delirium in mice, as well as the mechanism involved in delirium onset.

MATERIALS AND METHODS

Reagents

Scopolamine hydrobromide was purchased from Selleck Chemical (USA, S2508) and LPS from *E. coli* was purchased from Sigma-Aldrich (USA, L2630). All other chemicals and reagents were purchased from Sangon Biotech (China), unless otherwise specified.

Animals

All surgical and experimental procedures were approved by the Animal Care Committee of the State Key Laboratory of Biotherapy, Sichuan University, China, and were conducted following all institutional animal care and use committee guidelines (Approval No. K2018071). C57BL/6 mice (8 weeks of age, both sexes) were purchased from Hfk Bioscience (China) and housed in a specific pathogen-free facility at the State Key Laboratory of Biotherapy. The mice were allowed to adapt to the breeding environment for at least one week. The mice were housed in temperature-controlled rooms under a 12 h light-dark cycle, with water and food provided *ad libitum*. All recipient mice were randomly divided into groups using WPS Office (v2019, Kingsoft Office Software, China).

Animal models mimicking delirium

AS model (Peng et al., 2016): Anesthesia was started between 0700h and 0800h. Specifically, the mice were placed in a transparent acrylic chamber with 1.4% isoflurane (RWD Life Science Inc, China, R510-22-10) in 100% oxygen to simulate general anesthesia. Two hours after induction, the mice were removed from the chamber, and isoflurane anesthesia was maintained via a cone device. A longitudinal midline incision was made from the xiphoid to the 0.5 cm proximal pubic symphysis on the hairless skin, abdominal muscles, and peritoneum. The incision was then sutured layer by layer with a 5-0 absorbable surgical suture (Shinva, China, S29371T). The wound was then stitched, and the mice were kept warm with a heating pad (Deli, China, 10781603304) for 3–4 h post-surgery. Two AS model controls were established: i.e., mice given anesthesia alone (AA) and mice maintained under fasting and water deprivation conditions for 2 h (Control).

LPS injection model (Abraham & Johnson, 2009): LPS from *E. coli* was dissolved in 0.9% saline and intraperitoneally (i.p.) injected (0.33 mg/kg) into mice. Mice receiving a similar volume of 0.9% saline were used as the sham group (Sham-LPS).

Scop injection model (Qiu et al., 2016b): Scopolamine hydrobromide was dissolved in 0.9% saline and administered intraperitoneally (15 mg/kg) to mice. Mice receiving a similar volume of 0.9% saline were used as the sham group (Sham-Scop).

Behavioral tests

As the different models develop delirium-like phenotypes at different time points (Mouton et al., 2012; Peng et al., 2016; Qiu et al., 2016b; Schreuder et al., 2017), the time points used in this study were not consistent between models. For the AS model mice, behavioral tests were carried out 6 h and 24 h after treatment. For the LPS-injected mice, behavioral tests were carried out 2 h and 18 h post-injection. For the Scop-injected mice, behavioral tests were carried out 0.5 h and 6 h post-injection.

Two-trial recognition Y-maze test: The maze was made of white polymethylmethacrylate and consisted of identical three arms (5 cm wide, 35 cm long, 10 cm high) at 120° (SANS Biological Technology, China, SA204). Visual cues were placed on the walls of the maze. For the two-trial recognition Y-maze test, the three equal arms were randomly designated as the start arm, novel arm, and other arm using WPS Office (v2019, Kingsoft Office Software, China). The test process included two trials separated by a 1 h inter-trial interval, with all testing performed during the light phase of the circadian cycle. In the first trial (training), the mice were allowed to explore two arms (the start and other arm) for 10 min, with the novel arm blocked. In the second trial (retention), the mice were placed back in the maze in the same start arm and allowed to navigate for 5 min, with free access to all three arms. Behaviors were video recorded (Panasonic, Japan) during the 5 min trial, and the Supermaze^{TM} video-tracking system (v2.0, Xinruan, China) was used for analysis. Data were expressed as a percentage of duration of novel arm entries during the second 5 min trial.

Y-maze spontaneous alternation test: Each mouse was first placed in the center of the Y-maze mentioned above and allowed to explore freely for 8 min. The sequences and total number of arm entries were recorded. An arm entry was considered complete when the hind paws of the mouse were placed entirely within the arm. The alternation percentage was defined as the number of triads containing entries into all three arms divided by the maximum possible alternations (total

number of arms entered−2)×100).

Open field test: The open field is a square arena made of white polymethylmethacrylate (25 cm wide, 25 cm long, 25 cm high), divided into inner and outer fields (Med Associates Inc, USA, ENV-017M-27 and ENV-510S). The mouse was placed in the chamber for 5 min for acclimatization. Spontaneous exploration of three 16-beam IR arrays located on the field was then recorded for 1 h and analyzed using the default settings of Activity Monitor v7 (Med Associates Inc. USA, SOF-812). Data were expressed as ambulatory distance and trajectory.

Rotarod treadmill test: Motor coordination of the animals after operation and treatment was measured using a rotarod for mice (SANS Biological Technology, China, SA102) under accelerating rotor mode (4 to 40 r/min, with an acceleration of 7.2 r/min² for 6 min). The interval from when the animal mounted the rod to when it fell off was recorded as the retention time, and mice that lasted for 360 s on the accelerating rotating rod were recorded as survivors. The animals were subjected to three trials within a day, and mean duration on the rod was recorded to obtain stable baseline values.

Mouse tissue preparation

Mice were sacrificed by anesthetic overdose (2% chloral hydrate and 8% ethyl carbamate), followed by intracardial perfusion with ice-cold phosphate-buffered saline (PBS, 0.01 mol/L, pH 7.4). Brains were extracted and the hippocampus was isolated and stored at −80 °C before use. For immunohistochemistry, mice were intracardially perfused with ice-cold PBS (0.01 mol/L, pH 7.4), followed by 4% paraformaldehyde (PFA). Brains were extracted and kept in 4% PFA at 4 °C before use.

Synaptosome preparation

For hippocampal synaptosome preparation, two hippocampi from the same mouse were homogenized in 400 μL of Buffer A (10 mmol/L Tris-HCl, pH 7.4, 0.32 mol/L sucrose) supplemented with the protease inhibitor phenylmethylsulfonyl fluoride (PMSF) (Beyotime, China, ST507) on ice. Cell debris and nuclei were pelleted by centrifugation at 1 250 ×*g* for 10 min at 4 °C. The supernatants (S1) were collected and then centrifuged at 12 500 ×*g* for 20 min at 4 °C to obtain the crude synaptosomes in the pellet (P2). P2 was resuspended in 200 μL of Buffer A, with layering onto a Ficoll gradient containing 7% and 13% Ficoll 400 (Sigma, USA, F2637) and Buffer A. After centrifugation at 45 000 ×*g* for 45 min at 4 °C, synaptosomes were identified at the 7%/13% Ficoll interface. The interface was diluted with 400 μL of Buffer A and centrifuged at 45 000 ×*g* for 45 min at 4 °C to pellet the synaptosomes. The synaptosomes were resuspended in 5% sodium dodecyl sulfate (SDS) buffer and maintained at −80 °C before use. The SDS-soluble synaptosome purity was tested using immunoblotting against known markers for synaptic, mitochondrial, and cytoskeletal fractions in Supplementary Figure S1.

Immunoblotting

Samples were homogenized in cell lysis buffer (Beyotime, China, P0013) supplemented with the protease inhibitor PMSF (Beyotime, China, ST507) and centrifuged at 12 000 ×*g* for 30 min at 4 °C. The supernatant was collected, and total protein concentration was determined using a BCA protein assay kit (Beyotime, China, P0011). Equal amounts of protein were separated in 4%–12% bis-Tris gels with 3-(N-morpholino)propanesulfonic acid (MOPS) running buffer at 140 V for 1 h, then transferred to polyvinylidene fluoride (PVDF) membranes using the Trans-Blot system at 100 V for 1 h. The membranes were then washed with tris buffered saline with tween 20 (TBST) (0.02 mol/L, pH 8.0) for 5 min at room temperature (20 °C), shaken, blocked with 5% skim milk in TBST (0.02 mol/L, pH 8.0) for 1 h at room temperature, and incubated with primary antibodies diluted in TBST (0.02 mol/L, pH 8.0) overnight at 4 °C with shaking. The following day, the membranes were washed five times (5 min each) in TBST (0.02 mol/L, pH 8.0) and incubated with peroxidase-conjugated secondary antibodies diluted in TBST (0.02 mol/L, pH 8.0) for 120 min at room temperature with shaking. The membranes were then washed three times (20 min each) in TBST (0.02 mol/L, pH 8.0), developed with enhanced chemiluminescent (NCM Biotech, China, P10300), and visualized using ChemiScope 6100 (CLiNX, China). Chemiluminescence band intensity quantifications were performed using ImageJ (v1.53a, NIH, USA). In this study, the following antibodies were used (diluted in 0.02 mol/L TBST, pH 8.0): 1:1 000 for anti-PSD95 (Abcam, USA, ab18258); 1:1 000 for anti-synaptophysin (Millipore, USA, MAB5258-I); 1:1 000 for anti-GluR1 (Sigma-Aldrich, USA, AB1504); 1:1 000 for anti-NR1 (Abcam, USA, ab109182); 1:1 000 for anti-NR2A (Abcam, USA, ab124913); 1:1 000 for anti-NR2B (Merck Millipore, USA, AB1557P); 1:1 000 for anti-synapsin Ⅰ (Abcam, USA, ab64581); 1:1 000 for anti-CaMKⅡ (Cell Signaling Technology, USA, 3362); 1:1 000 for anti-phospho-CaMKⅡ(Ser286) (Abcam, USA, ab32678); 1:10 000 for anti-mouse Ig (Sigma-Aldrich, USA, A9044); 1:10 000 for anti-rabbit Ig (Sigma Aldrich, USA, A0545); and 1:10 000 for anti-β-actin (Sigma-Aldrich, USA, A5441). All uncropped images of western blots are shown in Supplementary Figure S2.

Immunohistochemistry

For c-fos protein (Fos) punctiform staining, which reflect neuronal activities ~ 1.5 h before each time point, the brains were extracted 2 h (Scop), 3.5 h (LPS), and 7.5 (AS) after treatments. The brains were kept in 4% PFA at 4 °C for 24 h, then removed to 30% sucrose, which was changed every 24 h until the tissue sank to the bottom. Coronal slices (30 μm thick) were immunostained using rabbit anti-Fos antibodies (Cell Signaling Technology, USA, 2250S). Immunostains were amplified with Alexa Fluor488-labeled goat anti-rabbit antibodies (Jackson ImmunoResearch Laboratories, USA, 111-545-144). Fully stained samples were imaged using a SLIDEVIEW VS200 research slide scanner (Olympus, Japan) with a 10× objective (numerical aperture, 0.5). Quantitative analysis of Fos expression was performed using ImageJ (v1.53a, NIH, USA) with default settings. Semiquantitative analyses of Fos expression were performed for all brain areas via visual inspection by two trained independent observers.

For Nissl staining and choline acetyltransferase (ChAT) immunohistochemical analysis, brains were kept in 4% PFA for three days. Coronal sections (3 μm) were cut after embedding in paraffin wax using a cryostat instrument (Leica, German, RM2125). The mounted sections were incubated in cresyl violet for 10 min at 25 °C or anti-ChAT (Abcam, USA, ab18736) overnight at 4 °C, followed by anti-rabbit biotinylated secondary antibody (Thermo Fisher Scientific, USA, 31460) and chromogenic substrate 3,3′-diaminobenzidine (Abcam, USA, ab64238). The sections were then dehydrated through

gradient alcohol (50%, 75%, 95%, and 100%) and cover-slipped with neutral balsam (Solarbio, China, 96949-21-2), followed by clearance in xylene. Fully stained samples were imaged using a Pannoramic MIDI Ⅱ (3DHISTECH, Hungary) with 20× objective (numerical aperture, 0.5). Three images per section were evaluated and quantified using the default settings in ImageJ (v1.53a, NIH, USA).

Electrophysiology

Long-term potentiation (LTP) was measured, as described previously (Chen et al., 2017). Mice were deeply anesthetized with urethane (1.5 g/kg) at onset of delirium-like syndrome (30 min) and transcardially perfused with artificial cerebral spinal fluid (ACSF) (in mmol/L: NaCl 124, KCl 2.8, NaH_2PO_4.H2O 1.25, $CaCl_2$ 2.0, $MgSO_4$ 1.2, Na-vitamin C 0.4, $NaHCO_3$ 26, Na-lactate 2.0, Na-pyruvate 2.0 and D-glucose 10.0, pH=7.4). The hippocampal slices were then coronally sectioned (400 μm) with a vibratome (Leica, Germany, VT1200S) with 95% O_2 and 5% CO_2, and incubated in ACSF for 2 h to 4 h at 35 °C. A bipolar stimulating electrode was placed at the Schaffer collaterals of dorsal hippocampus CA3 pyramidal neurons, and a recording pipette filled with ACSF was placed at the ipsilateral striatum radiatum of the hippocampal CA1 area. An input-output curve was measured at different current stimulations (0.05 to 0.4 mA) and test field excitatory postsynaptic potentials (fEPSPs) were evoked at a frequency of 0.05 Hz and stimulus intensity adjusted to around 50% of the maximal response size. After a 30 min stable baseline, theta burst stimulation (TBS) was given to induce LTP. TBS consisted of two trains of stimuli (at 20 s intervals), with each train composed of five bursts (four pulses at 100 Hz in each burst) at an inter-burst interval of 200 ms. Data acquisition was performed with PatchMaster (HEKA Elektronik, Germany, v2.73). The average of the three stimuli within 1 min was used for statistical analysis.

Statistical analysis

Data are shown as individual values. Statistical analysis was performed using GraphPad Prism (v8.0 for Windows, GraphPad Software, USA) and presented as mean±standard error of the mean (*SEM*). Statistical methods are described individually in the figure legends. *P*-values of less than 0.05 were considered significant.

RESULTS

Neuronal activity reduction in mouse models of delirium

Delirium induces brain network dysfunction (Rapazzini, 2016; Van Montfort et al., 2019; Young, 2017), which should be considered when modeling this disorder in mice. Neuronal activity is indicative of brain network functionality, and Fos is widely used as a neuronal activity marker following peripheral stimulation (Bullitt, 1990; Guo et al., 2018; Zhang et al., 2002). Based on unbiased semiquantitative analysis, we measured the number of Fos+ neurons in selected brain regions previously linked with delirium (Dixon et al., 2018; Kawano et al., 2018; Tsai et al., 2020; Van Montfort et al., 2019; Young, 2017).

Our results indicated that AS did not reproduce the brain network dysfunction phenotype observed in delirium. Compared with the Control and AA groups, AS had no additional impact on the number of Fos+ neurons across the brain (Table 1; Figure 1A). In contrast, the number of Fos+ neurons in the lateral orbital cortex (LO), cingulate cortex (Cg1&Cg2), agranular insular cortex (AIV), hippocampal CA1 region (CA1), and hippocampal CA3 region (CA3) was significantly lower in mice treated with LPS than in the Sham-LPS group (Table 1; Figure 1A). Fos+ neurons were also increased in the central amygdala (CeA), a region responsible for processing sensory information for emotional integration and aversive effects (Table 1; Figure 1A). In the Scop-treated mice, most brain regions examined, including the prefrontal cortex (PFC), LO, ventral orbital cortex (VO), Cg1&Cg2, AIV, CA1, and CA3, exhibited reduced Fos+ neuronal activity, indicating brain network dysfunction (Table 1; Figure 1A).

The PFC, Cg1&Cg2, hippocampus, and CeA regions are considered as hub nodes within the brain network associated with delirium (Dixon et al., 2018; Kaboodvand et al., 2018), Thus, these regions were selected for further analysis. Within the hippocampus, excitatory synapses in the CA3 region are decreased in delirium (Cursano et al., 2021), and thus were included in the analysis. Consistently, AS did not alter the number of Fos+ neurons, indicating limited impact on neuronal

Table 1 Semiquantitative analysis of Fos+ neurons in delirium-related brain regions

Region	Anesthesia with surgery			Lipopolysaccharide		Scopolamine	
	Control	AA	AS	Sham-LPS	LPS	Sham-Scop	Scop
PFC	++	++/+++	++/+++	++/+++	++	++/+++	+/++
LO	++/+++	++/+++	++/+++	++/+++	+/++	++/+++	+
VO	+/++/+++	+/++/+++	+/++/+++	++/+++	++	++/+++	+/++
Cg1&Cg2	++/+++	++/+++	++/+++	+++	++	+++	++
RSC	+++	+++	+++	+++	+++	+++	+++
PtA	++/+++	++/+++	++	++/+++	++	++/+++	++
AIV	++/+++	++/+++	+/++/+++	+++	+/++	+++	+/++
CeA	+/++	++	++	+/++	+++	++	++
CA1	++/+	++/+	++/+	++	+	++	+
CA3	++/+	++	++/+	++	+	++	+
MS	++/+	++/+	+/++	++	++/+	+++/++	+++/++

For each given region, number of Fos+ neurons was assigned on a four-point scale: (0), no Fos+ neuronal nuclei; (+), sparsely distributed Fos+ neuronal nuclei (0–50); (++), intermediate number of Fos+ neuronal nuclei (50–300); (+++), high number of Fos+ neuronal nuclei (300–1 000). Biological replicates were obtained from three to four mice, and for each mouse, results from three slices were averaged. Brain regions were labeled according to the Mouse Brain in Stereotaxic Coordinates Atlas (3rd Edition). PFC: Prefrontal cortex; LO: Lateral orbital cortex; VO: Ventral orbital cortex; Cg1&Cg2: Cingulate cortex (Cg1&Cg2); RSC: Retrosplenial cortex; PtA: Parietal association cortex; AIV: Agranular insular cortex; CeA: Central amygdala; CA1: Hippocampal CA1 region; CA3: Hippocampal CA3 region; MS: Medial septum.

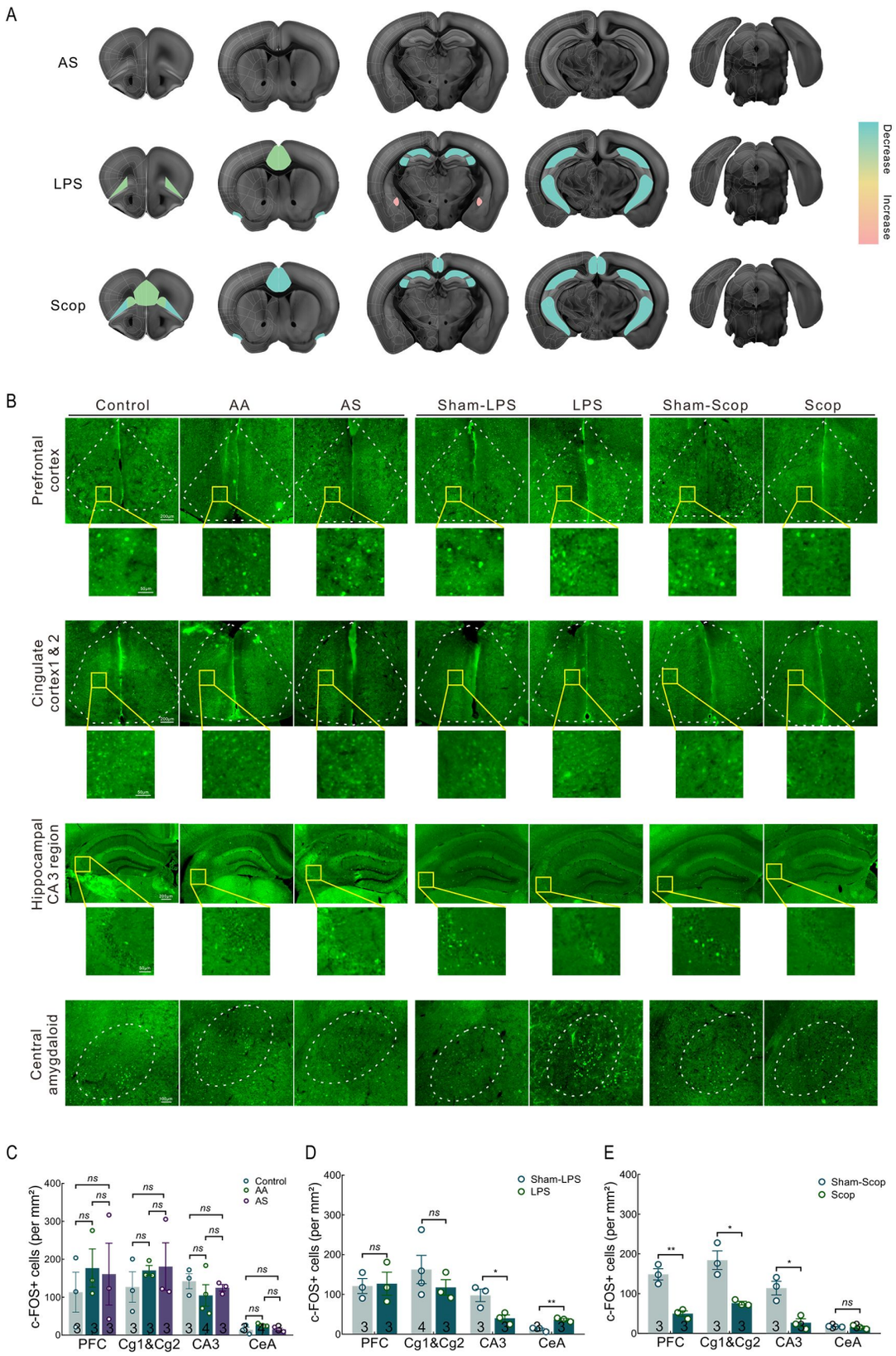

Figure 1 Quantification of Fos+ neuronal number in delirium-associated core brain regions

A: Representative heatmaps showing distribution of Fos (+) neurons in three delirium mouse models. Coronal plane shows mapped Fos expression signal overlaid on a reference atlas (adapted from Allen Mouse Brain Atlas) (Chon et al., 2019; Wang et al., 2020). B: Representative photomicrographs of Fos+ neurons in PFC, Cg1&Cg2, CA3, and CeA after treatments. Scale bars: 200 μm, 100 μm, and 50 μm, as indicated. C–E: Quantification of Fos+ neuronal number in PFC, Cg1&Cg2, CA3, and CeA after AA or AS treatment for 7.5 h (C), LPS treatment for 3.5 h (D), and Scop treatment for 2 h (E). *P*-values were calculated with *t*-test (LPS and Scop) or one-way analysis of variance (ANOVA) with *post-hoc* Tukey's multiple comparisons test (AA and AS): ns: No significance; *: $P<0.05$; **: $P<0.01$. *n* is shown in the bars. Error bars indicate *SEM*. PFC: Prefrontal cortex; Cg1&Cg2: Cingulate cortex; CA3: Hippocampal CA3 region; CeA: Central amygdala.

activity (Figure 1B, C). In contrast, LPS injection significantly lowered the number of Fos+ neurons in the CA3 region (LPS: 40 per μm² vs. Sham-LPS: 97 per μm², *P*=0.032), but induced a three-fold increase in the CeA (LPS: 37 per μm² vs. Sham-LPS: 6 per μm²; *P*=0.004, Figure 1B, D). No changes were detected in the PFC or Cg1&Cg2 after LPS treatment (Figure 1B, D). In comparison, the Scop-injected mice exhibited a reduction in Fos+ neurons in the PFC (Scop: 50 per μm² vs. Sham-Scop: 149 per μm²; *P*=0.003), Cg1&Cg2 (Scop: 76 per μm² vs. Sham-Scop: 184 per μm²; *P*=0.011), and CA3 (Scop: 27 per μm² vs. Sham-Scop: 114 per μm²; *P*=0.012, Figure 1B, E), indicating significant disruption in brain network function, mimicking observations in delirium patients.

Scop caused cognitive dysfunction without impairing locomotor function

Upon delirium onset after treatment, we assessed attention disturbance, a typical cognitive impairment in delirium (Association American Psychiatric, 2013), by detecting working memory lesions (Field et al., 2012; Murray et al., 2012; Skelly et al., 2019) using the Y-maze spontaneous alternation test (Figure 2A–D) and spatial memory (Kraeuter et al., 2019) using the two-trial recognition Y-maze test (Figure 2E–H).

In the Y-maze spontaneous alternation test, neither the AS group nor the AA group demonstrated a significant impact on working memory (Figure 2B). In contrast, the LPS-treated mice showed signs of working memory inhibition (LPS: 15.24% of alternation vs. Sham-LPS: 58.01%; *P*=0.004; Figure 2C). Similarly, the Scop-treated mice showed significantly impaired working memory (Scop: 22.43% vs. Sham-Scop: 55.06%, *P*=0.018; Figure 2D). Therefore, both LPS and Scop treatment can result in attention disturbance, mimicking human delirium phenotypes.

All three treatments impaired spatial memory (Figure 2F–H). While the Control group mice spent 50.4% of their spatial recognition time in the novel arm, this percentage decreased to 33.0% in the AA-treated mice (*P*=0.027) and 33.9% in the AS-treated mice (*P*=0.037). However, no differences were observed between the AA- and AS-treated mice (*P*=0.987, Figure 2F), indicating that spatial memory dysfunction was more likely related to the anesthesia procedure rather than follow-up surgery. Both the LPS- and Scop-treated mice spent significantly less time in the novel arm compared to their respective controls (LPS: *P*=0.014, Figure 2G; Scop: *P*=0.031, Figure 2H), indicating that both treatments caused a disturbance in awareness.

As the Y-maze is affected by locomotion disability (Prieur & Jadavji, 2019), we tested motor behaviors using the open field (Figure 2I–L) and rotarod treadmill tests (Figure 2M–R). Both the AS- and LPS-treated mice exhibited reduced locomotor activities, as evidenced by the reduced ambulatory distances of travel compared to their controls, which may have contributed to their Y-maze performances (Figure 2J–K). The AA- and AS-treated mice exhibited similar reductions in locomotor activities, again indicating that anesthesia may be the main factor affecting mouse behavior. However, the Scop-treated mice were hyperactive, as evidenced by the significantly prolonged travel distance (Figure 2L). Additional rotarod treadmill tests were conducted to examine compulsory motor functions, with no deficits found in any model (Figure 2M–O). This finding suggests that the decreased or increased motor activities observed in the open field test may reflect willingness rather than physical disability. Therefore, only the cognitive dysfunction observed in the Y-maze test under Scop treatment cannot be explained.

Cognitive impairments are reversible and associated with limited neuronal loss

One key feature of delirium is that its symptoms are transient and reversible, a critical distinction from dementia and other cognitive declines (Fong et al., 2015). To test whether the delirium mouse models met this criterion, we examined working and spatial memory at multiple time points.

Consistent with the clinical presentation of delirium, both working and spatial memory impairment recovered spontaneously in all models (Figure 3A–F). When tested 24 h after the AS procedure (vs. 6 h shown in Figure 2B, F), the mice showed no significant differences compared to the controls in Y-maze spontaneous alternation test (Figure 3A) and two-trial recognition Y-maze test performance (Figure 3D). Similarly, the LPS- and Scop-treated mice also showed recovery in the same cognitive tests (Figure 3B, C, E, F).

The transient cognitive impairment observed above indicates that no permeant neuronal loss occurred in the models. Therefore, we further evaluated the loss of neurons in delirium-related core brain regions (PFC, Cg1&Cg2, CeA, and CA3) using Nissl staining. Results showed that none of the treatments resulted in neuronal loss (Figure 4A–D), consistent with the spontaneous recovery in mice.

Cholinergic deficiency has long been considered a key participant in the pathogenesis of delirium, as impaired neurotransmission of acetylcholine in the brain is associated with typical changes in attention, cognition, and emotion among patients with delirium (Hshieh et al., 2008; Ruxton et al., 2015). As such, we measured the density of cholinergic neurons in the medial septum (MS), an important node of the cholinergic network, using ChAT staining. Consistent with total neuron counting, comparable levels of cholinergic neurons (ChAT-positive) were found in all mouse models of delirium (Figure 4E–J). These observations indicate that the reversible cognitive impairment seen in mice may not be mediated by direct neuronal loss.

Potential synaptic dysfunction may be responsible for reversible cognitive impairment

Given the lack of neuronal loss, it is likely that synaptic function was affected by the various treatments. We purified the synaptosome-enriched fraction of the hippocampus and analyzed the subcellular distribution of synaptic proteins by immunoblotting. Upon the manifestation of delirium-like behaviors after Scop treatment, the SDS fractions derived from the synaptosomes exhibited reduced stable anchoring of NR2A and phosphorylation of CaMKII at position 286 (NR2A: *P*=0.017; p-CaMKII: *P*=0.023; p-CaMKII/CaMKII: *P*=0.032, Figure 5C), indicating altered synaptic plasticity. Of note, synaptic protein abundance differed between the synaptosomes and total protein. Both AS and LPS treatment did not significantly change the abundance of synaptic proteins in the synaptosomes compared to their respective controls (Figure 5A, B). However, both treatments significantly reduced PSD95 abundance in total extracts of the hippocampus (Supplementary Figure S3). To further confirm the impacts on synaptic plasticity, we examined the effect of the Scop-induced model on LTP in CA3–CA1 synapses. Consistent with the neuroethological phenotypes, Scop-

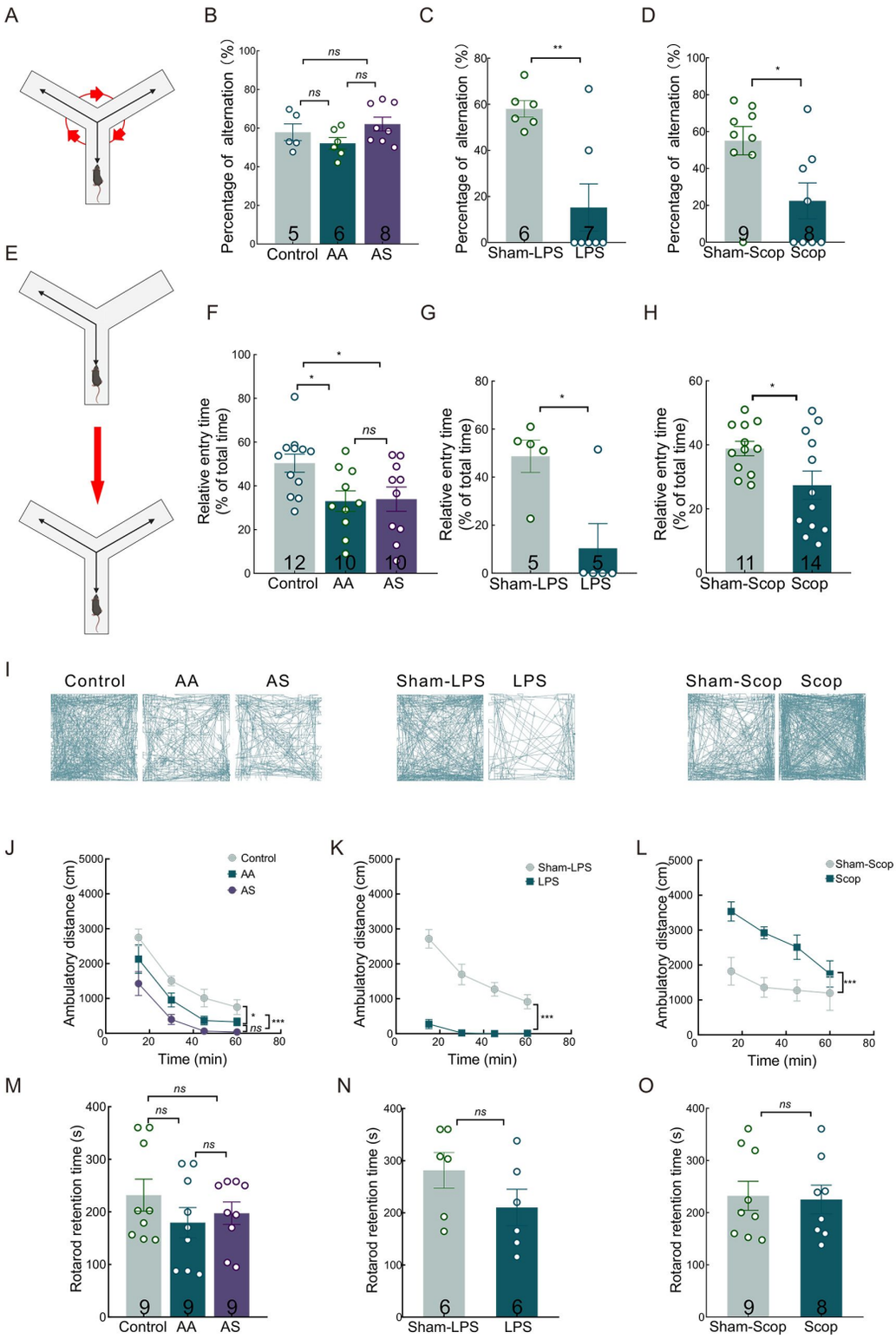

Figure 2 Cognitive and locomotor function tests indicate delirium-like phenotypes

A: Schematic of Y-maze spontaneous alternation test. B–D: Percentage of alternation in Y-maze spontaneous alternation test after AA or AS treatment for 6 h (B), LPS treatment for 2 h (C), and Scop treatment for 0.5 h (D). E: Schematic of two-trial recognition Y-maze test. F–H: Relative duration time in novel arm in two-trial recognition test after AA or AS treatment for 6 h (F), LPS treatment for 2 h (G), and Scop treatment for 0.5 h (H). I: Example of mouse trajectory between 5.5 h and 6.5 h after AA or AS treatment (left), 1.5 and 2.5 h after LPS treatment (middle), and 0 and 1 h after Scop treatment (right). J–L: Ambulatory travel distance in open field test between 5.5 h and 6.5 h after AA or AS treatment (J), 1.5 h and 2.5 h after LPS treatment (K), and 0 and 1 h after Scop treatment (L). For Control, AA, and AS: *n*=9; For Sham-LPS and LPS: *n*=8; For Sham-Scop: *n*=8. M–O: Latency to fall in rotarod treadmill test after AS and AA treatment for 6 h (M), LPS treatment for 2 h (N), and Scop treatment for 0.5 h (O). For J–L, *P*-values were calculated with two-way analysis of variance (ANOVA) for all mouse models. For all other figures, *P*-values were calculated with *t*-test (LPS and Scop) or one-way ANOVA with *post-hoc* Tukey's multiple comparisons test (AA and AS): ns: No significance; *: $P<0.05$; **: $P<0.01$; ***: $P<0.001$. *n* is shown in bars unless otherwise specified. Error bars indicate *SEM*.

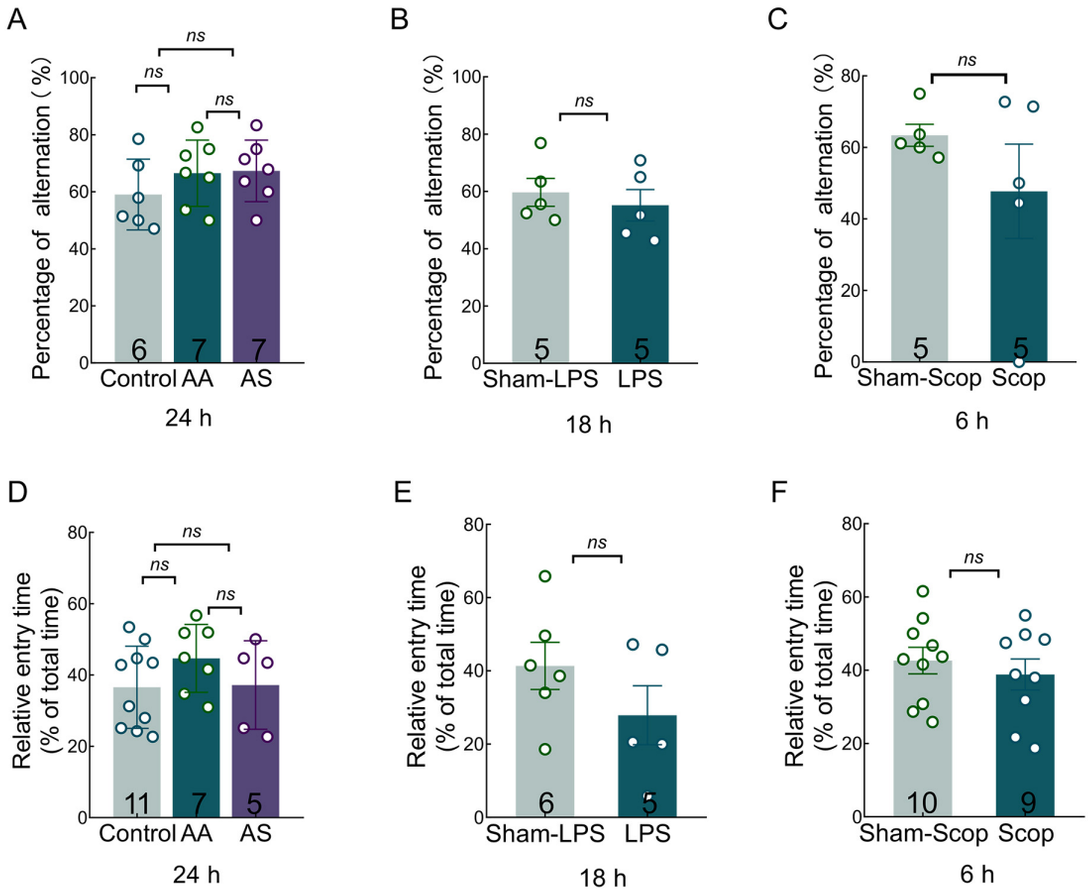

Figure 3 Prolonged cognitive function tests after treatments

A–C: Percentage of alternation in Y-maze spontaneous alternation test after AA or AS treatment for 24 h (A), LPS treatment for 18 h (B), and Scop treatment for 6 h (C). D–F: Relative duration time in novel arm in two-trial recognition test after AA or AS treatment for 24 h (D), LPS treatment for 18 h (E), and Scop treatment for 6 h (F). *P*-values were calculated with *t*-test (LPS and Scop) or one-way analysis of variance (ANOVA) with *post-hoc* Tukey's multiple comparisons test (AA and AS): ns: No significance. *n* is shown in bars. Error bars indicate *SEM*.

injected model mice failed to induce LTP at 3–4 h after treatment and showed improvement at 5–6 h after treatment (3–4 h: *P*=0.033; 5–6 h: *P*=0.807, Figure 5D, E). These results suggest that Scop induces delirium-like syndrome through acute effects on synaptic plasticity.

DISCUSSION

The DSM-5 depicts delirium as an evident disturbance in attention and awareness, associated with cognitive impairment in memory (Association American Psychiatric, 2013). Modeling delirium in mice still represents a challenge as the most characteristic symptoms, such as confused thinking and reduced awareness, cannot be recapitulated. The current strategy to develop models mimicking delirium involves introducing susceptible factors observed in patients into mice. Studies focusing on animal models with specific etiologies are considered crucial for identifying the biological factors that play a causal role in surpassing critical thresholds and triggering delirium (Wilson et al., 2020). In the current study, we found that a single-dose injection of Scop effectively reproduced the clinical features of delirium, including reversible memory deficits, disrupted neuronal network, hyperactivity without motor dysfunction, and synaptic dysfunction without neuronal loss. This unique combination of characteristics distinguishes the mice from models of AD and other cognitive impairments, which is crucial for future studies on its mechanism of action and therapeutic development. The other models of delirium induced by AS or bacterial LPS injection only partially manifested the clinical features of delirium.

As a functional brain disorder, delirium can result from coordinated dysfunction of the neural network rather than discrete pathological lesions. Prior functional magnetic resonance imaging (fMRI) studies examining the brains of patients with delirium have revealed complex disruption in the internal connectivity of the anterior default mode network (DMN), dysfunction of the saline network (SN), and reduction in the connectivity of the DMN and SN with key nodes of the frontoparietal control network (FPCN) (Rapazzini, 2016; Van Montfort et al., 2019; Young, 2017). Brain regions related to brain networks include the PFC, LO, and VO within the FPCN (Dixon et al., 2018), parietal association cortex (PtA), Cg1&Cg2, and retrosplenial cortex (RSC) within the DMN region (Ferrier et al., 2020; Kaboodvand et al., 2018; Raichle, 2015), and the AIV within the SN (Tsai et al., 2020). The CA1, CA3, and CeA regions, which receive dense cholinergic projections from the MS to aid in the regulation of spatial memory, anxiety, and emotional memory, are also related to delirium (Li et al., 2018; Schäble et al., 2012). Combining the features of neurobehavioral syndromes and impaired neural networks, delirium may result from the disruption of neuronal activity secondary to systemic disturbances (Greenwood &

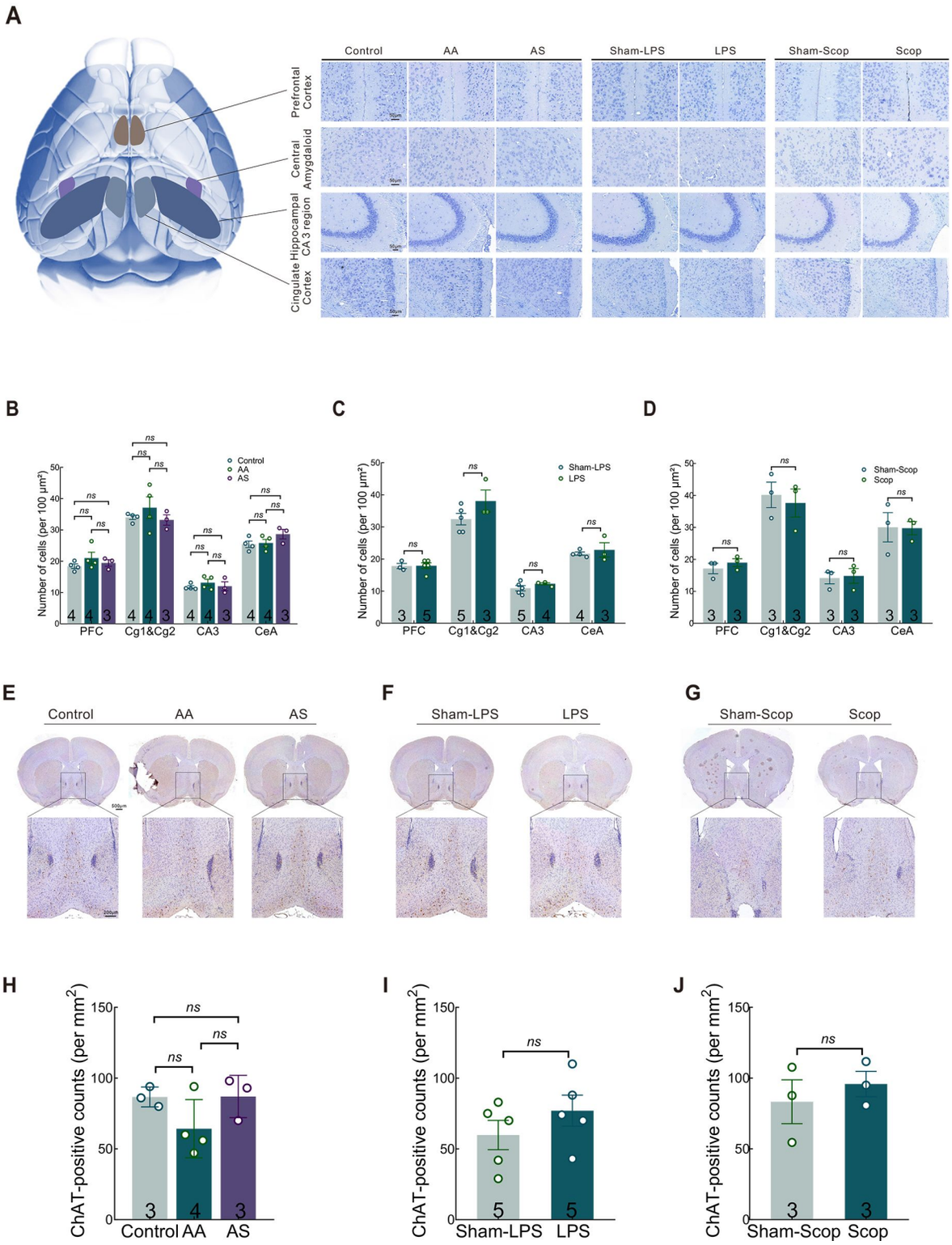

Figure 4 Neuropathological changes in delirium-related brain regions

A: Schematic of ventral brain view and representative photomicrographs of Nissl-staining after different treatments. Distinct regions are depicted in different colors. Scale bar, 50 μm, as indicated. B–D: Quantifications of Nissl-stained neuron numbers in typical regions after AA or AS treatment for 6 h (B), LPS treatment for 2 h (C), and Scop treatment for 0.5 h (D). E–G: Representative photomicrographs showing anti-ChAT staining after different treatments. Scale bar: 500 μm and 200 μm, as indicated. H–J: Quantifications of numbers of anti-ChAT-stained neurons in MS. *P*-values were calculated with *t*-test (LPS and Scop) or one-way analysis of variance (ANOVA) with *post-hoc* Tukey's multiple comparisons test (AA and AS): ns: No significance. *n* is shown in bars. Error bars indicate *SEM*.

Parasuraman, 2010; Leonard et al., 2015; Maldonado, 2013; Shafi et al., 2017). Thus, we hypothesized that delirium may decrease the expression of c-fos, an indication of fewer Fos+ neurons, to reduce neuronal activity in brain regions affected by delirium (Tulogdi et al., 2012). In this study, we explored animal models of delirium from the perspective of neuronal

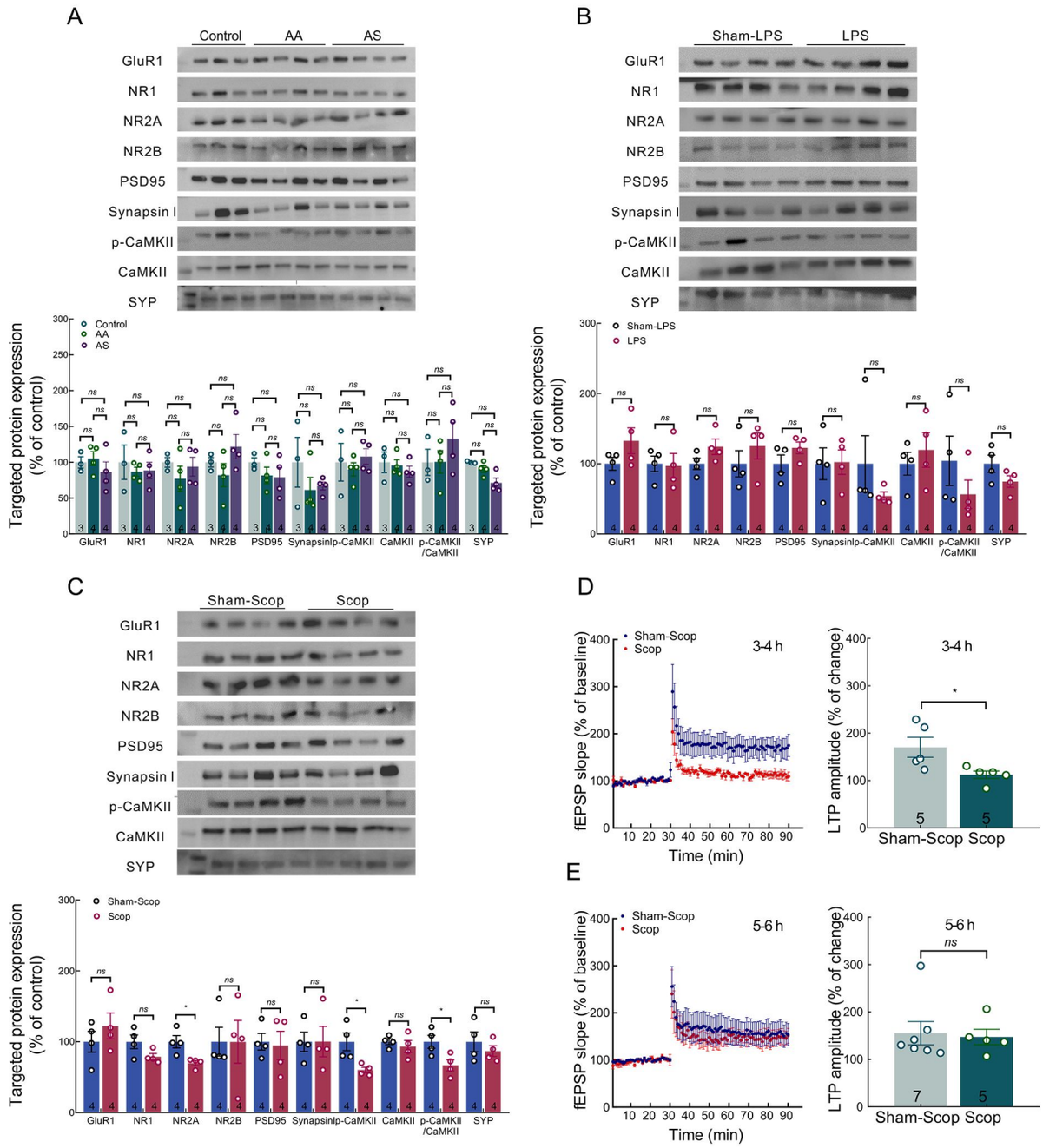

Figure 5 Hippocampal synaptic protein expression after treatments and LTP after Scop treatment

A–C: Representative images (top) and quantifications (bottom) showing immunoblot analysis of synaptic proteins α-amino-3-hydroxy-5-methyl-4-isoxazolepropionate receptor subunits glutamate receptor 1 (GluR1), *N*-methyl-D-aspartate receptor subunit glutamate receptor 1 (NR1), *N*-methyl-D-aspartate receptor subunit glutamate receptor 2a (NR2A), *N*-methyl-D-aspartate receptor subunit glutamate receptor 2b (NR2B), postsynaptic density-95 (PSD95), calcium-calmodulin (CaM)-dependent protein kinase II (CaMKII), p-CaMKII, synaptophysin (SYP), and synapsin I in hippocampal synaptosomes of mice after AS treatment for 6 h (A), LPS treatment for 2 h (B), and Scop treatment for 0.5 h (C). D, E: Time course of normalized f-EPSP slope values (left) and quantifications between 50–60 min (right) in brain slices at 3–4 h (D) or 5–6 h (E) post Scop treatment. *P*-values were calculated with *t*-test (LPS and Scop) or one-way analysis of variance (ANOVA) with *post-hoc* Tukey's multiple comparisons test (AA and AS): ns: No significance; *: $P<0.05$; **: $P<0.01$. *n* is shown in bars. Error bars indicate *SEM*.

activity in the brain network, providing insights into integrated research aimed at examining the neural networks underlying delirium.

Previous studies have attributed cognitive decline to hypothermia, postoperative pain, and infection following surgical procedures (Kawano et al., 2018; Zhang et al., 2016), with AS thus considered a model for delirium. While aged mice are more susceptible to surgery and memory decline (Kawano et al, 2018), we found that AS failed to mediate working memory deficits in young adult mice, and that spatial memory impairment was primarily linked to anesthesia. Anesthesia alone is known to cause cognitive dysfunction, i.e., POCD. Delirium post-surgery and POCD are both defined as perioperative neurocognitive disorders (PND) (Evered & Silbert, 2018). However, unlike delirium, POCD clinically manifests as mild cognitive decline in one or more cognitive

domains (Berger et al., 2018; Daiello et al., 2019; Monk & Price, 2011), and is generally associated with anesthesia (Mason et al., 2010). In mice, general anesthesia induced by sevoflurane and isoflurane is also commonly used to induce spatial memory dysfunction to mimic POCD (Ge et al., 2021). Thus, anesthesia-induced memory decline may not be specific to delirium.

Acute peripheral inflammatory stimulation induces neuronal activation, proinflammatory cytokine expression, and inflammatory mediator release (Cerejeira et al., 2014). Delirium is a common manifestation of multiple organ dysfunction in the context of systemic challenge by bacterial endotoxins (Siami et al., 2008). In adult rodents, single-dose LPS can induce cognitive deficits in Morris water-maze and Y-maze tests within 48 h (Lee et al., 2008; Richwine et al., 2009). In our study, we found that LPS treatment also affected neuronal activities in the AIV, hippocampus, and CeA, potentially contributing to memory and attention deficits (Bressler & Menon, 2010; Tsai et al., 2020). However, systemic inflammation also induced severe inactivity in mice, interfering with the performance of the cognitive and memory tests. Therefore, drawing conclusive results from the Y-maze (or other cognitive impairment tests) becomes challenging, as they heavily rely on the motivation and willingness of mice to complete the tasks.

Muscarinic cholinergic antagonists, such as Scop, can uniquely produce hallucinations, forming a subclass of hallucinogens known as “deliriants” (Lakstygal et al., 2019). Here, we found that a single dose of Scop (15 mg/kg) induced reversible cognitive impairment in mice. Notably, Scop administration reduced neuronal activities in the PFC, Cg1&Cg2, and AIV, brain regions highly correlated with memory and consciousness (Buckner et al., 2008; Ferrier et al., 2020; Oh et al., 2019; Van Montfort et al., 2018). A medium dosage of Scop (3 mg/kg) has been reported to result in disruptions in DMN functional connectivity within 30 min (Shah et al., 2016). Scop intoxication is characterized by a slowed electroencephalogram (EEG) power spectrum and low coherence at the alpha and beta frequencies (Sloan et al., 1992; Thomas et al., 2008). In our study, the dose used induced deficits in specific brain regions, and unlike its intoxication, the observed phenotypes were reversible and not dependent on neuronal loss. The latter factor is important as this model has been suggested as a psychopharmacological model of AD (Bajo et al., 2015), a disease with significant neuronal loss and non-reversible memory deficits. The delirium phenotypes observed in our study were largely reversible, consistent with clinical findings. However, it is important to note that delirium also serves as an independent risk factor for AD (Davis et al., 2017), suggesting that even short-term brain dysfunction may accumulate and contribute to long-term irreversible brain impairment. It is speculated that delirium duration elicits neurochemical alterations in the brain, increasing its vulnerability to stressors that can trigger dementia (Fong et al., 2020). Furthermore, in contrast to AS and LPS treatment, Scop caused hyperactivity in mice. According to the DSM-5, delirium can be divided into several motor subtypes, e.g., hyperactive, hypoactive, and mixed. Our findings suggest that Scop may trigger hyperactive delirium-like phenotypes.

Synaptic pathology likely plays a role in altered connectivity, although neuronal loss is minimal in most cortical regions of delirium brains (Sanders, 2013). Our study provided preliminary evidence to support that cholinergic synaptic functions may be responsible for the observed memory dysfunction. Unlike Scop, neither surgery nor LPS directly inhibit cholinergic receptor function, but both appear to affect synaptic functions through an imbalance in cholinergic receptors (Wang et al., 2022; Zivkovic et al., 2015). We found that Scop decreased CaMKII phosphorylation and NR2A abundance in hippocampal synaptosomes, both of which participate in LTP. We further found a time-dependent impairment of LTP with Scop treatment, consistent with the synaptosome findings. Anesthesia and LPS treatment can cause a time-dependent decline in PSD95 expression in the hippocampus (Gao et al., 2021; Khan et al., 2018; Muhammad et al., 2019). Here, we observed a significant reduction in PSD95 levels in total protein extracts at 2 h after LPS treatment, which occurred at a faster rate compared to the proteasome-mediated pathways (Ehlers, 2003). These findings suggest that LPS treatment may expedite the PSD95 turnover rate in the hippocampus. Considering the alterations in synaptic proteins and LTP, postsynaptic membrane plasticity may play a key role in mediating the behavioral changes observed in various delirium models.

In conclusion, we compared different models of delirium using clinically relevant assessments. Our results showed that Scop injection in mice induced a reversible hyperactive delirium-like phenotype without causing neuronal loss but accompanied by changes in neuronal activity. These findings provide valuable insights for future mechanistic studies of delirium in animal models and may contribute to the development of potential therapies for delirium.

SUPPLEMENTARY DATA

Supplementary data to this article can be found online.

COMPETING INTERESTS

The authors declare that they have no competing interests.

AUTHORS’ CONTRIBUTIONS

P.L. conceived of the study. P.L. and J.R.Y. raised funds for the study. Q.W. and X.Z. designed and performed the experiments with supervision from P.L. and J.R.Y. Y.Y.P. and J.J.L. performed the electrophysiological experiments, J.F.W., B.T.Z., and J.X.T. performed immunohistochemical analysis with supervision from Y.J.G. and P.L. Y.L.Z., Y.Y.J., and J.M. performed animal surgeries with Q.W. Q.W., J.R.Y., and P.L. integrated the data and wrote the draft manuscript. All authors read and approved the final version of the manuscript.

REFERENCES

Abraham J, Johnson RW. 2009. Central inhibition of interleukin-1β ameliorates sickness behavior in aged mice. *Brain, Behavior, and Immunity*, **23**(3): 396−401.

Association American Psychiatric. 2013. Diagnostic and Statistical Manual of Mental Disorders: DSM-5. 5th ed. Washington: American Psychiatric Publishing.

Bajo R, Pusil S, López ME, et al. 2015. Scopolamine effects on functional brain connectivity: a pharmacological model of Alzheimer’s disease. *Scientific Reports*, **5**(1): 9748.

Berger M, Terrando N, Smith SK, et al. 2018. Neurocognitive function after cardiac surgery: from phenotypes to mechanisms. *Anesthesiology*, **129**(4): 829−851.

Bressler SL, Menon V. 2010. Large-scale brain networks in cognition: emerging methods and principles. *Trends in Cognitive Sciences*, **14**(6): 277−290.

Buckner RL, Andrews-Hanna JR, Schacter DL. 2008. The brain's default network: anatomy, function, and relevance to disease. *Annals of the New York Academy of Sciences*, **1124**(1): 1−38.

Bullitt E. 1990. Expression of *C-fos*-like protein as a marker for neuronal activity following noxious stimulation in the rat. *The Journal of Comparative Neurology*, **296**(4): 517−530.

Cerejeira J, Firmino H, Vaz-Serra A, et al. 2010. The neuroinflammatory hypothesis of delirium. *Acta Neuropathologica*, **119**(6): 737−754.

Cerejeira J, Lagarto L, Mukaetova-Ladinska EB. 2014. The immunology of delirium. *Neuroimmunomodulation*, **21**(2–3): 72–78.

Chan MTV, Cheng BCP, Lee TMC, et al. 2013. BIS-guided anesthesia decreases postoperative delirium and cognitive decline. *Journal of Neurosurgical Anesthesiology*, **25**(1): 33−42.

Chen L, Huang ZL, Du YH, et al. 2017. Capsaicin attenuates amyloid-β-induced synapse loss and cognitive impairments in mice. *Journal of Alzheimer's Disease*, **59**(2): 683−694.

Chen WN, Yeong KY. 2020. Scopolamine, a toxin-induced experimental model, used for research in Alzheimer's disease. *CNS, Neurological Disorders-Drug Targets*, **19**(2): 85−93.

Choi SH, Lee H, Chung TS, et al. 2012. Neural network functional connectivity during and after an episode of delirium. *The American Journal of Psychiatry*, **169**(5): 498−507.

Chon U, Vanselow DJ, Cheng KC, et al. 2019. Enhanced and unified anatomical labeling for a common mouse brain atlas. *Nature Communications*, **10**(1): 5067.

Cursano S, Battaglia CR, Urrutia-Ruiz C, et al. 2021. A CRHR1 antagonist prevents synaptic loss and memory deficits in a trauma-induced delirium-like syndrome. *Molecular Psychiatry*, **26**(8): 3778−3794.

Daiello LA, Racine AM, Yun Gou R, et al. 2019. Postoperative delirium and postoperative cognitive dysfunction: overlap and divergence. *Anesthesiology*, **131**(3): 477−491.

Davis DHJ, Muniz-Terrera G, Keage HAD, et al. 2017. Association of delirium with cognitive decline in late life: a neuropathologic study of 3 population-based cohort studies. *JAMA Psychiatry*, **74**(3): 244−251.

Dixon ML, De La Vega A, Mills C, et al. 2018. Heterogeneity within the frontoparietal control network and its relationship to the default and dorsal attention networks. *Proceedings of the National Academy of Sciences of the United States of America*, **115**(7): E1598−E1607.

Ehlers MD. 2003. Activity level controls postsynaptic composition and signaling via the ubiquitin-proteasome system. *Nature Neuroscience*, **6**(3): 231−242.

Evered LA, Silbert BS. 2018. Postoperative cognitive dysfunction and noncardiac surgery. *Anesthesia & Analgesia*, **127**(2): 496−505.

Ferrier J, Tiran E, Deffieux T, et al. 2020. Functional imaging evidence for task-induced deactivation and disconnection of a major default mode network hub in the mouse brain. *Proceedings of the National Academy of Sciences of the United States of America*, **117**(26): 15270−15280.

Field RH, Gossen A, Cunningham C. 2012. Prior pathology in the basal forebrain cholinergic system predisposes to inflammation-induced working memory deficits: reconciling inflammatory and cholinergic hypotheses of delirium. *The Journal of Neuroscience*, **32**(18): 6288−6294.

Fleischmann R, Traenkner S, Kraft A, et al. 2019. Delirium is associated with frequency band specific dysconnectivity in intrinsic connectivity networks: preliminary evidence from a large retrospective pilot case-control study. *Pilot and Feasibility Studies*, **5**(1): 2.

Fong TG, Davis D, Growdon ME, et al. 2015. The interface between delirium and dementia in elderly adults. *The Lancet Neurology*, **14**(8): 823−832.

Fong TG, Vasunilashorn SM, Ngo L, et al. 2020. Association of Plasma Neurofilament Light with Postoperative Delirium. *Annals of Neurology*, **88**(5): 984−994.

Gao SN, Zhang SY, Zhou HM, et al. 2021. Role of mTOR-regulated autophagy in synaptic plasticity related proteins downregulation and the reference memory deficits induced by anesthesia/surgery in aged mice. *Frontiers in Aging Neuroscience*, **13**: 628541.

Ge X, Zuo Y, Xie JH, et al. 2021. A new mechanism of POCD caused by sevoflurane in mice: cognitive impairment induced by cross-dysfunction of iron and glucose metabolism. *Aging*, **13**(18): 22375−22389.

Goldberg TE, Chen C, Wang YJ, et al. 2020. Association of delirium with long-term cognitive decline: a meta-analysis. *JAMA Neurology*, **77**(11): 1373−1381.

Greenwood PM, Parasuraman R. 2010. Neuronal and cognitive plasticity: a neurocognitive framework for ameliorating cognitive aging. *Frontiers in Aging Neuroscience*, **2**: 150.

Guo YJ, Tang X, Zhang JC, et al. 2018. Corticosterone signaling and a lateral habenula–ventral Tegmental area circuit modulate compulsive self-injurious behavior in a rat model. *The Journal of Neuroscience*, **38**(23): 5251−5266.

Hshieh TT, Fong TG, Marcantonio ER, et al. 2008. Cholinergic deficiency hypothesis in delirium: a synthesis of current evidence. *The Journals of Gerontology:Series A*, **63**(7): 764−772.

Inouye SK, Westendorp RG, Saczynski JS. 2014. Delirium in elderly people. The *Lancet*, **383**(9920): 911–922.

Itil T, Fink M. 1966. Anticholinergic drug-induced delirium: experimental modification, quantitative EEG and behavioral correlations. *Journal of Nervous and Mental Disease*, **143**(6): 492−507.

Kaboodvand N, Bäckman L, Nyberg L, et al. 2018. The retrosplenial cortex: a memory gateway between the cortical default mode network and the medial temporal lobe. *Human Brain Mapping*, **39**(5): 2020−2034.

Kawano T, Yamanaka D, Aoyama B, et al. 2018. Involvement of acute neuroinflammation in postoperative delirium-like cognitive deficits in rats. *Journal of Anesthesia*, **32**(4): 506−517.

Khan A, Ali T, Rehman SU, et al. 2018. Neuroprotective effect of quercetin against the detrimental effects of LPS in the adult mouse brain. *Frontiers in Pharmacology*, **9**: 1383.

Kraeuter AK, Guest PC, Sarnyai Z. 2019. The Y-maze for assessment of spatial working and reference memory in mice. *In*: Guest PC. Pre-Clinical Models: Techniques and Protocols. New York: Humana Press, 105–111.

Krewulak KD, Stelfox HT, Leigh JP, et al. 2018. Incidence and prevalence of delirium subtypes in an Adult ICU: a systematic review and meta-analysis. *Critical Care Medicine*, **46**(12): 2029−2035.

Lakstygal AM, Kolesnikova TO, Khatsko SL, et al. 2019. DARK classics in chemical neuroscience: atropine, scopolamine, and other anticholinergic deliriant hallucinogens. *ACS Chemical Neuroscience*, **10**(5): 2144−2159.

Lee JW, Lee YK, Yuk DY, et al. 2008. Neuro-inflammation induced by lipopolysaccharide causes cognitive impairment through enhancement of beta-amyloid generation. *Journal of Neuroinflammation*, **5**(1): 37.

Leonard M, Adamis D, Saunders J, et al. 2015. A longitudinal study of delirium phenomenology indicates widespread neural dysfunction. *Palliative and Supportive Care*, **13**(2): 187−196.

Li XN, Yu B, Sun QT, et al. 2018. Generation of a whole-brain atlas for the cholinergic system and mesoscopic projectome analysis of basal forebrain cholinergic neurons. *Proceedings of the National Academy of Sciences of the United States of America*, **115**(2): 415−420.

Li YJ, Chen DT, Wang HB, et al. 2021. Intravenous versus volatile anesthetic effects on postoperative cognition in elderly patients undergoing laparoscopic abdominal surgery. *Anesthesiology*, **134**(3): 381−394.

Maldonado JR. 2013. Neuropathogenesis of delirium: review of current etiologic theories and common pathways. *Proceedings of the National Academy of Sciences of the United States of America Psychiatry*, **21**(12): 1190−1222.

Mason SE, Noel-Storr A, Ritchie CW. 2010. The impact of general and

regional anesthesia on the incidence of post-operative cognitive dysfunction and post-operative delirium: a systematic review with meta-analysis. *Journal of Alzheimer's Disease*, **22**(Suppl 3): S67−S79.

Monk TG, Price CC. 2011. Postoperative cognitive disorders. *Current Opinion in Critical Care*, **17**(4): 376−381.

Mouton PR, Kelley-Bell B, Tweedie D, et al. 2012. The effects of age and lipopolysaccharide (LPS)-mediated peripheral inflammation on numbers of central catecholaminergic neurons. *Neurobiology of Aging*, **33**(2): 423.e27−423.e36.

Muhammad T, Ikram M, Ullah R, et al. 2019. Hesperetin, a citrus flavonoid, attenuates LPS-induced neuroinflammation, apoptosis and memory impairments by modulating TLR4/NF-κB signaling. *Nutrients*, **11**(3): 648.

Murray C, Sanderson DJ, Barkus C, et al. 2012. Systemic inflammation induces acute working memory deficits in the primed brain: relevance for delirium. *Neurobiology of Aging*, **33**(3): 603−616.e3.

Neufeld KJ, Yue JR, Robinson TN, et al. 2016. Antipsychotic medication for prevention and treatment of delirium in hospitalized adults: a systematic review and meta-analysis. *Journal of the American Geriatrics Society*, **64**(4): 705−714.

O'Connor JC, Lawson MA, André C, et al. 2009. Lipopolysaccharide-induced depressive-like behavior is mediated by indoleamine 2, 3-dioxygenase activation in mice. *MolecularPsychiatry*, **14**(5): 511−522.

Oh ES, Fong TG, Hshieh TT, et al. 2017. Delirium in older persons: advances in diagnosis and treatment. *JAMA*, **318**(12): 1161−1174.

Oh J, Shin JE, Yang KH, et al. 2019. Cortical and subcortical changes in resting-state functional connectivity before and during an episode of postoperative delirium. *Australian & New Zealand Journal of Psychiatry*, **53**(8): 794−806.

Peng M, Zhang C, Dong YL, et al. 2016. Battery of behavioral tests in mice to study postoperative delirium. *Scientific Reports*, **6**: 29874.

Prieur EAK, Jadavji NM. 2019. Assessing spatial working memory using the spontaneous alternation Y-maze test in aged male mice. *Bio-Protocol*, **9**(3): e3162.

Qiu YM, Chen DM, Huang XJ, et al. 2016a. Neuroprotective effects of HTR1A antagonist WAY-100635 on scopolamine-induced delirium in rats and underlying molecular mechanisms. *BMC Neuroscience*, **17**(1): 66.

Qiu YM, Huang XJ, Huang LN, et al. 2016b. 5-HT(1A) receptor antagonist improves behavior performance of delirium rats through inhibiting PI3K/Akt/mTOR activation-induced NLRP3 activity. *IUBMB Life*, **68**(4): 311−319.

Raichle ME. 2015. The brain's default mode network. *Annual Review of Neuroscience*, **38**: 433−447.

Rapazzini P. 2016. Functional interrelationship of brain aging and delirium. *Aging Clinical and Experimental Research*, **28**(1): 161−164.

Richwine AF, Sparkman NL, Dilger RN, et al. 2009. Cognitive deficits in interleukin-10-deficient mice after peripheral injection of lipopolysaccharide. *Brain, Behavior, and Immunity*, **23**(6): 794−802.

Rozzini R, Inzoli M, Trabucchï M. 1988. Delirium from transdermal scopolamine in an elderly woman. *JAMA*, **260**(4): 478.

Ruxton K, Woodman RJ, Mangoni AA. 2015. Drugs with anticholinergic effects and cognitive impairment, falls and all-cause mortality in older adults: a systematic review and meta-analysis. *British Journal of Clinical Pharmacology*, **80**(2): 209−220.

Salluh JIF, Wang H, Schneider EB, et al. 2015. Outcome of delirium in critically ill patients: systematic review and meta-analysis. *BMJ*, **350**: h2538.

Sanders RD. 2013. Delirium, neurotransmission, and network connectivity: the search for a comprehensive pathogenic framework. *Anesthesiology*, **118**(3): 494−496.

Schäble S, Huston JP, De Souza Silva MA. 2012. Neurokinin$_2$-R in medial septum regulate hippocampal and amygdalar Ach release induced by intraseptal application of neurokinins A and B. *Hippocampus*, **22**(5): 1058−1067.

Schreuder L, Eggen BJ, Biber K, et al. 2017. Pathophysiological and behavioral effects of systemic inflammation in aged and diseased rodents with relevance to delirium: a systematic review. *Brain, Behavior, and Immunity*, **62**: 362−381.

Shafi MM, Santarnecchi E, Fong TG, et al. 2017. Advancing the neurophysiological understanding of delirium. *Journal of the American Geriatrics Society*, **65**(6): 1114−1118.

Shah D, Blockx I, Keliris GA, et al. 2016. Cholinergic and serotonergic modulations differentially affect large-scale functional networks in the mouse brain. *Brain Structure and Function*, **221**(6): 3067−3079.

Siami S, Annane D, Sharshar T. 2008. The encephalopathy in sepsis. *Critical Care Clinics*, **24**(1): 67−82.

Skelly DT, Griffin ÉW, Murray CL, et al. 2019. Acute transient cognitive dysfunction and acute brain injury induced by systemic inflammation occur by dissociable IL-1-dependent mechanisms. *Molecular Psychiatry*, **24**(10): 1533−1548.

Sloan EP, Fenton GW, Standage KP. 1992. Anticholinergic drug effects on quantitative electroencephalogram, visual evoked potential, and verbal memory. *Biological Psychiatry*, **31**(6): 600−606.

Thomas C, Hestermann U, Kopitz J, et al. 2008. Serum anticholinergic activity and cerebral cholinergic dysfunction: an EEG study in frail elderly with and without delirium. *BMC Neuroscience*, **9**: 86.

Trzepacz PT, Leavitt M, Ciongoli K. 1992. An animal model for delirium. *Psychosomatics*, **33**(4): 404−415.

Tsai PJ, Keeley RJ, Carmack SA, et al. 2020. Converging structural and functional evidence for a rat salience network. *Biological Psychiatry*, **88**(11): 867−878.

Tulogdi Á, Sörös P, Tóth M, et al. 2012. Temporal changes in c-Fos activation patterns induced by conditioned fear. *Brain Research Bulletin*, **88**(4): 359−370.

Van Den Biggelaar AHJ, Gussekloo J, De Craen AJM, et al. 2007. Inflammation and interleukin-1 signaling network contribute to depressive symptoms but not cognitive decline in old age. *Experimental Gerontology*, **42**(7): 693−701.

Van Montfort SJT, Van Dellen E, Stam CJ, et al. 2019. Brain network disintegration as a final common pathway for delirium: a systematic review and qualitative meta-analysis. *NeuroImage:Clinical*, **23**: 101809.

Van Montfort SJT, Van Dellen E, Van Den Bosch AMR, et al. 2018. Resting-state fMRI reveals network disintegration during delirium. *NeuroImage:Clinical*, **20**: 35−41.

Wang Q, Ding SL, Li Y, et al. 2020. The Allen Mouse Brain Common Coordinate Framework: A 3D Reference Atlas. *Cell*, **181**(4): 936−953.e920.

Wang TH, Xu GP, Zhang X, et al. 2022. Malfunction of astrocyte and cholinergic input is involved in postoperative impairment of hippocampal synaptic plasticity and cognitive function. *Neuropharmacology*, **217**: 109191.

Wilson JE, Mart MF, Cunningham C, et al. 2020. Delirium. *Nature Reviews Disease Primers*, **6**(1): 90.

Young JWS. 2017. The network model of delirium. *Medical Hypotheses*, **104**: 80−85.

Zhang JH, Zhang DS, McQuade JS, et al. 2002. *C-fos* regulates neuronal excitability and survival. *Nature Genetics*, **30**(4): 416−420.

Zhang MD, Barde S, Yang T, et al. 2016. Orthopedic surgery modulates neuropeptides and BDNF expression at the spinal and hippocampal levels. *Proceedings of the National Academy of Sciences of the United States of America*, **113**(43): E6686−E6695.

Zivkovic AR, Sedlaczek O, Von Haken R, et al. 2015. Muscarinic M1 receptors modulate endotoxemia-induced loss of synaptic plasticity. *Acta Neuropathologica Communications*, **3**: 67.